Aerodynamic Performance of the 2018 InSight Mars Lander

Ashley M. Korzun*, Robert W. Maddock†, Mark Schoenenberger‡, Karl T. Edquist§, and Carlie H. Zumwalt¶
NASA Langley Research Center, Hampton, VA, 23681, USA

Christopher D. Karlgaard‖
Analytical Mechanics Associates, Hampton, VA, 23666, USA

InSight touched down in Elysium Planitia on 26 November 2018, becoming NASA's eighth successful entry, descent, and landing (EDL) at Mars. InSight was a build-to-print of the successful 2008 Phoenix EDL system, flying a non-spinning, ballistic trajectory with a 70-degree sphere-cone aeroshell (2.65 meter diameter), disk-gap-band parachute, and pulsed terminal descent and landing engines. This work discusses entry aerodynamic performance for InSight up to parachute deployment, including pre-flight aerodynamics predictions and comparisons with post-flight reconstruction, as well as comparisons with the Phoenix reconstruction.

I. Nomenclature

C_A	=	axial force coefficient
CG	=	center of gravity
C_l	=	rolling moment coefficient
C_m	=	pitching moment coefficient
C_{m_q}	=	pitch damping coefficient
C_N	=	normal force coefficient
C_n	=	yawing moment coefficient
C_{n_r}	=	yaw damping coefficient
C_Y	=	side force coefficient
D	=	capsule diameter, m
Kn	=	Knudsen number
M	=	Mach number
T	=	total condition
V	=	atmosphere-relative velocity, m/s
X, Y, Z	=	capsule coordinates from nose, m
α	=	angle of attack, deg
β	=	angle of sideslip, deg
γ	=	inertial flight path angle, deg
σ	=	standard deviation
∞	=	freestream condition

II. Introduction

On 26 November 2018, the Interior Exploration using Seismic Investigations (InSight) lander touched down in Elysium Planitia, becoming NASA's eighth successful entry, descent, and landing (EDL) at Mars. The stationary lander contains a suite of instruments designed to study the interior structure of Mars [1]. InSight was a build-to-print of the successful 2008 Phoenix EDL system, flying a non-spinning, unguided, ballistic trajectory with a 70° sphere-cone

*Research Aerospace Engineer, Atmospheric Flight and Entry Systems Branch, M/S 489 Hampton, VA 23681, Member AIAA.
†Aerospace Engineer, Atmospheric Flight and Entry Systems Branch, M/S 489 Hampton, VA 23681, Senior Member AIAA.
‡Aerospace Engineer, Atmospheric Flight and Entry Systems Branch, M/S 489 Hampton, VA 23681, Senior Member AIAA.
§Aerospace Engineer, Atmospheric Flight and Entry Systems Branch, M/S 489 Hampton, VA 23681, AIAA Fellow.
¶Aerospace Engineer, Atmospheric Flight and Entry Systems Branch, M/S 489 Hampton, VA 23681, Member AIAA.
‖Supervising Engineer, Atmospheric Flight and Entry Systems Branch, M/S 489 Hampton, VA 23681, AIAA Fellow.

aeroshell, supersonic disk-gap-band parachute, and pulsed terminal descent and landing engines. Figure 1 describes the nominal EDL concept of operations for InSight. This paper focuses on the aerodynamic performance of the entry capsule, prior to parachute deployment.

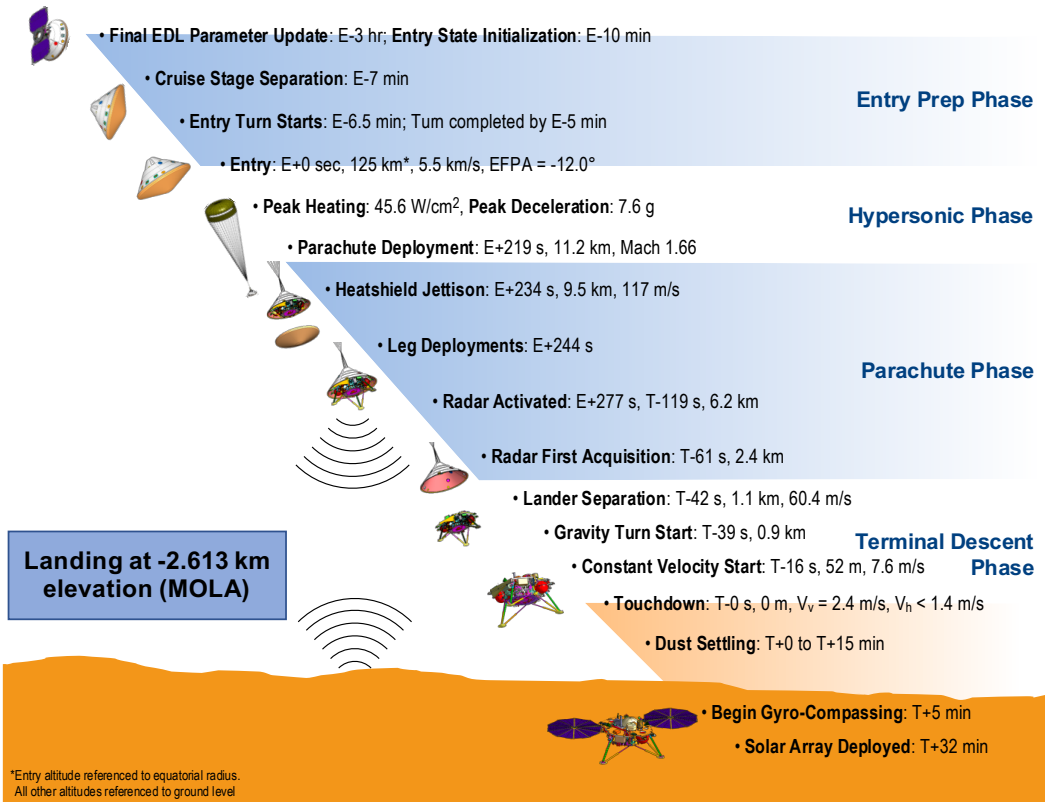

Fig. 1 Nominal InSight EDL timeline of events.

InSight successfully satisfied all EDL performance requirements, though several metrics were at either the high or low end of pre-flight predictions [2]. Specifically, the vehicle experienced a peak deceleration of 8.3 Earth g, where the predicted 99^{th} %-tile magnitude was 8.1 g (system requirement was 13 g). Additionally, the EDL time of flight was 41 s shorter than predicted (6m29s predicted vs. 5m48s reconstructed). InSight touched down 12.3 km uprange and 6.1 km crossrange of the target landing site in Elysium Planitia. Complete details on trajectory and atmosphere reconstruction are provided by Karlgaard et al. [3], and the post-flight performance assessment is discussed by Maddock et al. [2]. As InSight did not fly any instrumentation, such as a Flush-Air Data System (FADS), capable of separating aerodynamics from atmosphere, all reconstruction has been completed using the nominal aerodynamics database described in this paper.

The remainder of this paper is organized as follows. Section III describes the pre-flight aerodynamics database and dispersions used to quantify flight performance prior to parachute deployment. Section IV discusses the InSight as-flown aerodynamic performance, with comparisons to the predicted nominal as well as Phoenix as-flown performance, and contributions to the departures from pre-flight predicted performance.

III. Pre-Flight Aerodynamics Predictions

This section describes the InSight entry capsule, aerodynamics database, and uncertainties applied in Monte Carlo trajectory analyses.

A. Vehicle Geometry and Reference Trajectory

The EDL systems for InSight and Phoenix (PHX) are in-family with those used on prior, Viking-heritage vehicles, with many similarities to Mars Pathfinder (MPF) and the Mars Exploration Rovers (MER), as summarized in Table 1.

Similar to all Mars EDL capsules flown to date, InSight flew a rigid aeroshell with a 70° sphere-cone forebody and a conical aftbody (Fig. 2). This aeroshell removes in excess of 99% of the vehicle's kinetic energy prior to deployment of the supersonic parachute. Blunt body hypersonic aerodynamics are characterized by the forebody geometry, whereas the aftbody geometry becomes increasingly significant as the vehicle decelerates through supersonic conditions. While both Phoenix and InSight flew with an on-board 3-axis reaction control system (RCS), due to uncertainty in the potential for control reversal in the implemented RCS design and to reduce risk, the control system deadbands were widened during the hypersonic entry phase to reduce the likelihood of firings within the atmosphere [4]. InSight did not experience any RCS firings during EDL.

Table 1 Comparison of in-family EDL at Mars

	1997 MPF	2004 MER-A	2004 MER-B	2008 PHX	2018 InSight
V_{entry} (km/s, inertial)	7.26	5.4	5.5	5.6	5.8
γ_{entry} (deg, inertial)	-14.06	-11.49	-11.47	-13.01	-12.0
Ballistic coefficient (kg/m^2)	63	94	94	65	69
Entry mass (kg)	584	827	832	573	608
Entry attitude control	2 RPM passive	2 RPM passive	2 RPM passive	3-axis RCS*	3-axis RCS*
Heatshield diameter (m)	2.65	2.65	2.65	2.65	2.65
α_{trim} (deg)	0	0	0	0	0
Touchdown mass (kg)	360	539	539	350	375
Elevation (km MOLA)	-2.5	-1.9	-1.4	-4.1	-2.6

*RCS dead-banded within the atmosphere

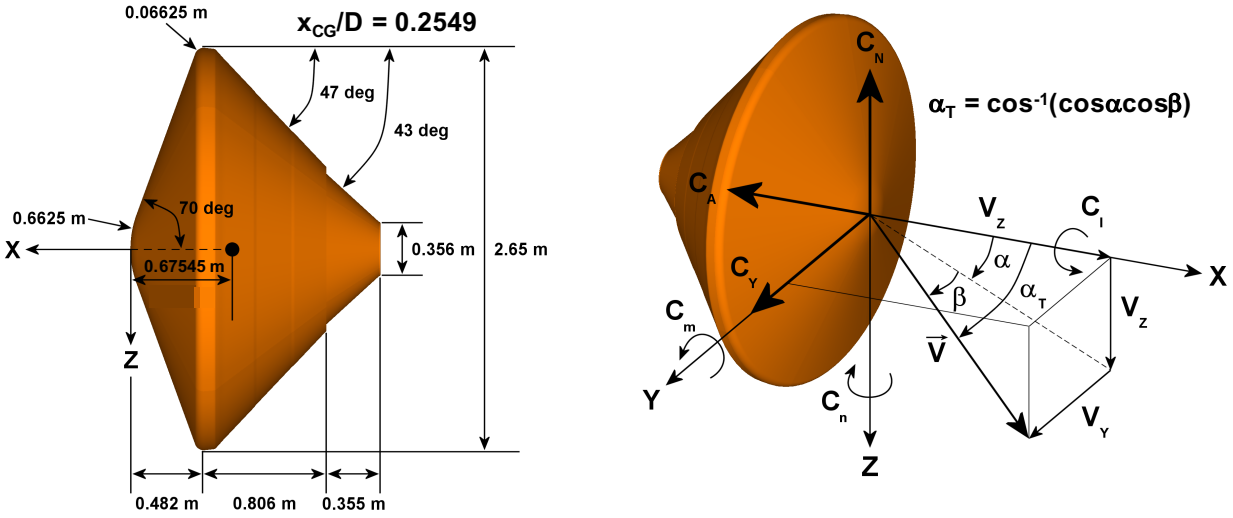

Fig. 2 InSight capsule geometry and aerodynamics coordinate frame.

The aerodynamics database for InSight was identical to that developed for Phoenix [5]. Though InSight was a heavier vehicle packaged into the same size aeroshell, the entry velocity and entry flight path angle were similar, at 5.8 km/s and -12.0° for InSight and 5.6 km/s and -13.0° for Phoenix, respectively. Figure 3 shows the comparison between the Phoenix design reference trajectory, originally used to develop the nominal Phoenix aerodynamics database, and the 2018 InSight nominal trajectory. Hypersonic non-equilibrium chemistry effects are primarily dependent on density and velocity. For Phoenix, a sensitivity study was done for a ±20% variation in atmospheric density at a given velocity, showing this variation produced less than an 0.1% change in C_A [5].

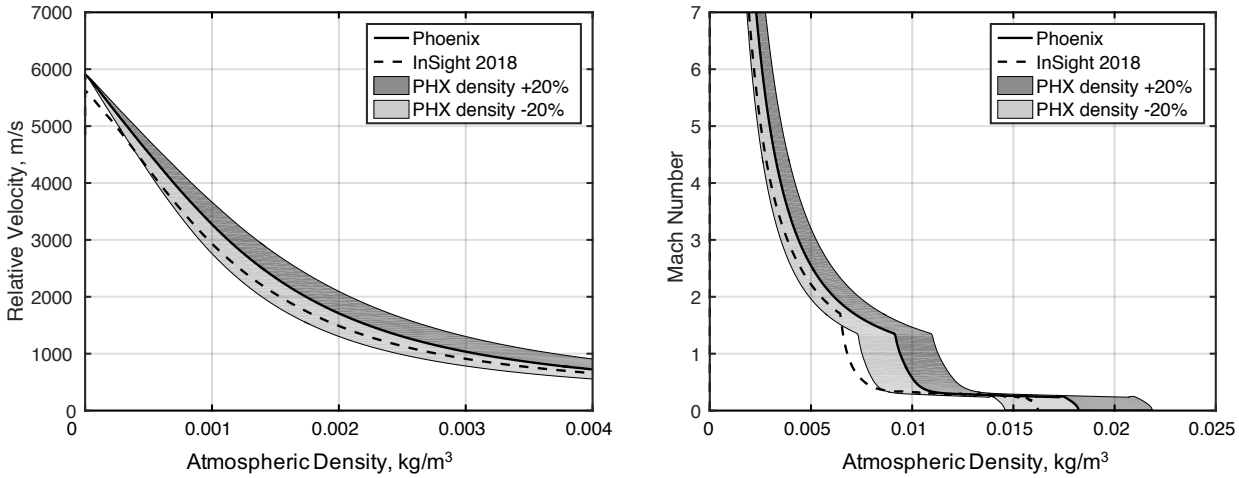

Fig. 3 Phoenix design reference and InSight nominal trajectories.

The aerodynamics database was built using computational methods and best practices originally established for Mars Pathfinder and data from the Mars Exploration Rover and Viking programs. Inputs to the aerodynamics database are angle of attack (α), angle of sideslip (β), Knudsen number (Kn), atmosphere-relative velocity (V_∞), and Mach number (M_∞). Aerodynamic coefficients are specified by total angle of attack, α_T, and relevant flight regime (free-molecular, transitional, hypersonic, supersonic, and transonic), as the different flow physics in each regime requires a different testing or analysis approach to generate aerodynamic force and moment coefficients [5]. Figure 2 shows the aerodynamic coordinate frame. Table 2 summarizes the regime definitions and ranges of conditions included within the InSight aerodynamics database. The following sections provide a brief summary of the nominal aerodynamics database. Detailed discussion on the development of the aerodynamics database can be found in Ref. [5].

Table 2 Static aerodynamics flight regimes

Flight Regime	Range of Applicability	Input Parameters	Method
Free-Molecular	$Kn > 1000$ $0° < \alpha_T < 180°$	α, β	MER DAC free [6]
Transitional	$0.00106 < Kn < 1000$ $0° < \alpha_T < 180°$	Kn, α, β	MER DSMC [6]
Hypersonic	$Kn < 0.00106$ and $M_\infty > 8.8$ $0° < \alpha_T < 16°$	V_∞, α, β	LAURA (forebody) [5]
Supersonic	$2 < M_\infty < 6.3$ $0° < \alpha_T < 16°$	M_∞, α, β	LAURA (forebody + $\Delta C_{A,base}$)
Transonic	$0.4 < M_\infty < 1.5$ $0° < \alpha_T < 16°$	M_∞, α, β	Viking wind tunnel [7]

B. Static Aerodynamics

The static aerodynamics database for InSight was unchanged from that used for Phoenix. High-altitude (non-continuum) coefficients, as well as dynamic damping characteristics, were taken from MER testing and analysis. Hypersonic static coefficients were generated with non-equilibrium Navier-Stokes computational fluid dynamics (CFD). Supersonic static coefficients were developed using CFD on the forebody and a Viking-derived pressure correction for aftbody contributions [5].

For blunt bodies, C_A dominates the aerodynamic forces on the vehicle ($C_A >> C_N$). Figure 4 shows the points

along the design reference trajectory comprising the aerodynamics database, as well as the data for C_A. These data are functions of α, β and either Kn, V_∞, or M_∞, depending on the regime of flight. As expected, C_A is greatest at low angles of attack, with this trend persisting as the vehicle decelerates until near Mach 1.5. At low supersonic conditions and below, the pressure on the backshell of the vehicle contributes an increment to the pressure that is a less strong function of angle of attack. Once the parachute is deployed, nominally near Mach 1.7, the parachute forces and moments dominate the vehicle's dynamics.

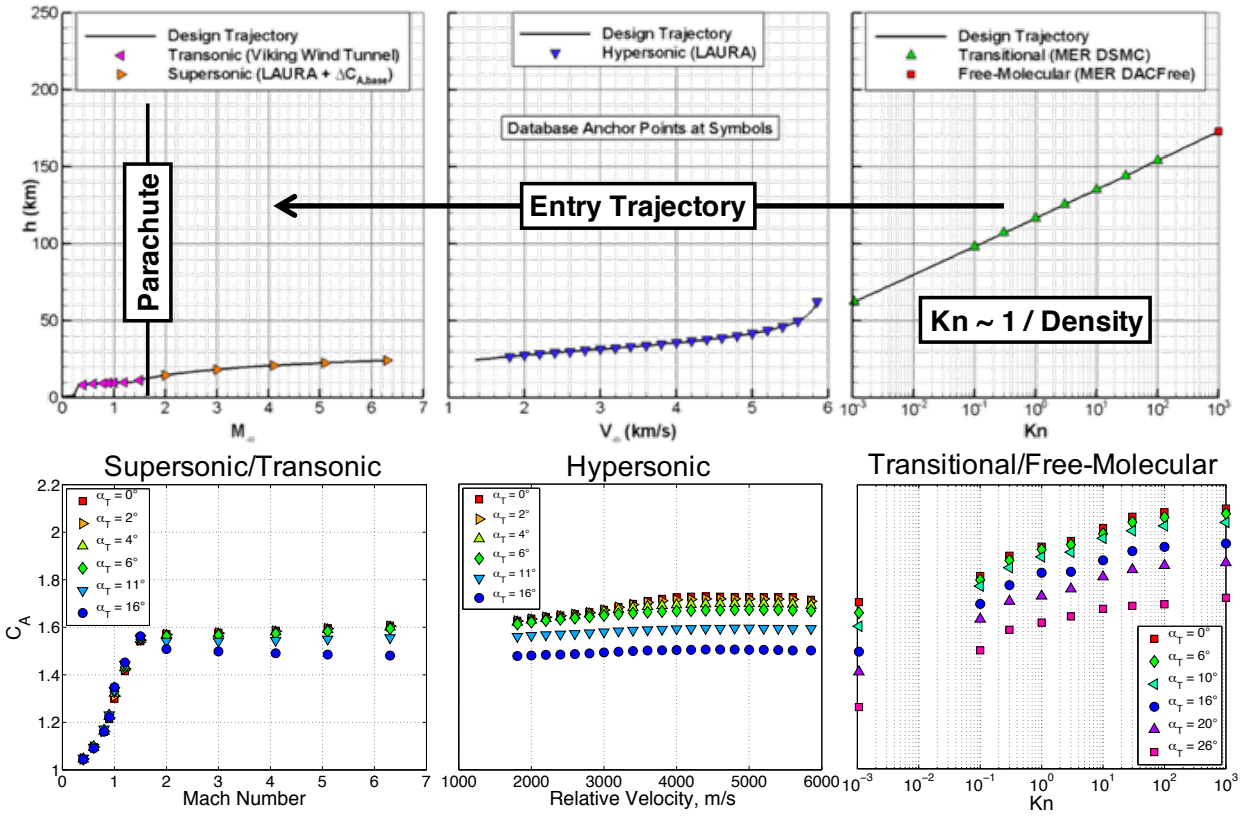

Fig. 4 Axial force coefficient database [5].

As predicted and subsequently observed in prior ballistic Mars entries, including Pathfinder [8], MER [6], and Phoenix [5], the 70° sphere-cone geometry flying through a non-equilibrium CO_2 environment at hypersonic conditions is characterized by regions of bounded static instability due to a shift in the sonic line from the nose of the vehicle to the shoulder and back to the nose. The vehicle is statically unstable when the slope of $\delta C_{m,CG}/\delta\alpha$ is positive. Shown in Fig. 5, static instabilities were predicted in two regions along the reference trajectory: one near the non-continuum / continuum boundary and the other later in the hypersonic phase, between 3800 and 3300 m/s. At these conditions, the vehicle, though axisymmetric and having no radial center-of-gravity (CG) offset, is predicted to trim at a non-zero angle of attack as a result of non-equilibrium chemistry effects on the vehicle heatshield pressure distribution. The impact of these effects on both InSight and Phoenix is described in Section IV.

C. Dynamic Pitch Damping

Figure 6 shows the InSight dynamic damping database, based on the MER ballistic-range pitch damping model [5]. Blunt body geometries like that flown on InSight are characteristically dynamically unstable at supersonic conditions. Pitch oscillations are undamped, and vehicle attitude and attitude rate growth as the vehicle decelerates through these conditions have the potential to jeopardize deployment and inflation of the supersonic parachute. As shown in Fig. 6, the vehicle is assumed to be neutrally stable at free-molecular conditions ($C_{m_q} = C_{n_r} = 0$). At hypersonic continuum conditions, the vehicle is dynamically stable ($C_{m_q} < 0$). Between free-molecular and hypersonic conditions, C_{m_q} values are computed as a function of Kn with a bridging function. The vehicle is dynamically unstable ($C_{m_q} > 0$) for $M_\infty < 3.5$,

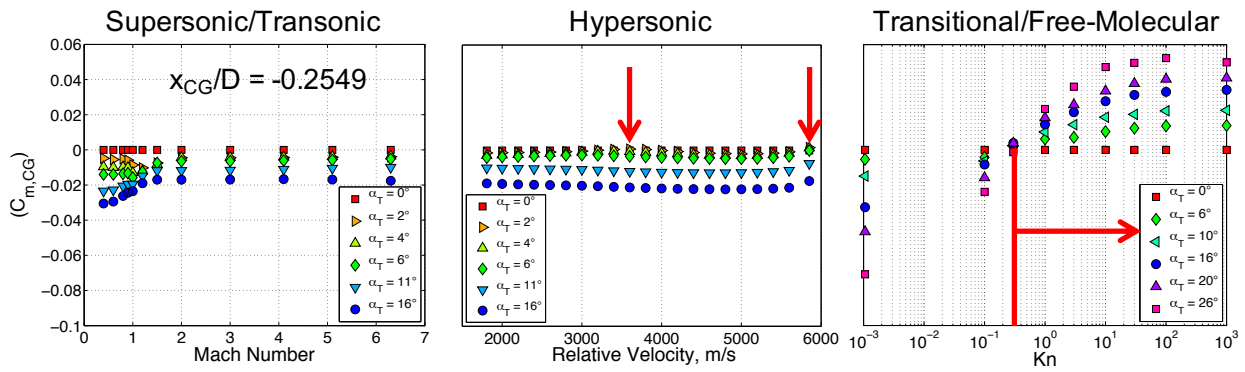

Fig. 5 Pitching moment coefficient database [5], with static instabilities indicated by red arrows.

starting with small angles of attack. For M_∞ < 1.5, the vehicle is dynamically unstable for all angles of attack within the database (0° to 16°).

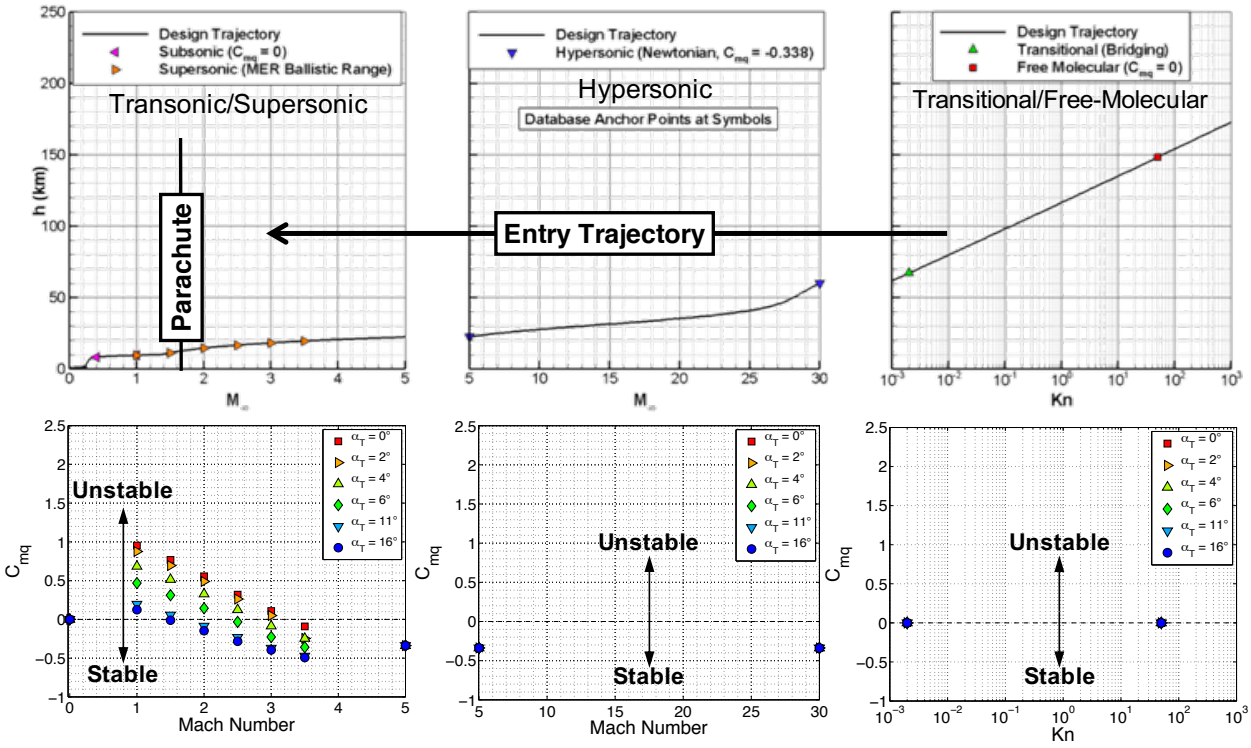

Fig. 6 Dynamic damping database [5].

D. Capsule Aerodynamics Dispersions

Aerodynamics uncertainties were unchanged from Phoenix, deriving heritage from Mars Pathfinder and MER [5]. Similar to the composition of the nominal aerodynamics database, the uncertainties are also delineated by flow regime, as shown in Table 3. The uncertainties are applied to the aerodynamic coefficients decomposed into the vehicle body frame (see Fig. 2), and all moments are dispersed about the vehicle's center of gravity, not the moment reference point (center of the vehicle heatshield). The differences in uncertainty magnitude reflect differences in fidelity and uncertainty in the underlying tools and methods used to generate the nominal aerodynamic coefficients, as well as engineering judgement and post-flight reconstruction on prior Mars EDL missions [5, 6, 8]. For all static coefficients other than axial

force, uncertainties are applied as separately dispersed adders and multipliers, permitting the trim attitude (intercept) and stability (slope) to be dispersed independently. The uncertainty in C_{m_q} is correlated with that in C_{n_r}; all other uncertainties are uncorrelated. All static aerodynamics uncertainties are applied assuming a normal distribution. For dynamic aerodynamics uncertainties, at hypersonic conditions, uncertainties are applied assuming a normal distribution, and at supersonic and transonic conditions, uncertainties are applied assuming a uniform distribution.

Table 3 InSight and Phoenix aerodynamics dispersions

Static Aerodynamics (Uncorrelated)

Flight Regime	C_A	C_N, C_Y	C_m, C_n	C_l
Transitional / Free-Molecular $Kn > 0.1$	±5%	±0.01, ±20%	±0.005, ±20%	1.24×10^{-6}
Hypersonic $M_\infty < 10$	±3%	±0.01, ±20%	±0.003, ±20%	1.24×10^{-6}
Supersonic $1.5 < M_\infty < 5$	±10%	±0.01, ±20%	±0.005, ±20%	1.24×10^{-6}
Transonic $0.4 < M_\infty < 1.5$	±10%	1.25 × Supersonic	1.25 × Supersonic	1.24×10^{-6}

Dynamic Damping (Correlated)

Flight Regime	C_{m_q}	C_{n_r}
Transitional / Free-Molecular $Kn > 0.1$	±0.15	±0.15
Hypersonic $M_\infty > 6$	±0.15	±0.15
Supersonic $1.5 < M_\infty < 3$	+0.5 × [2.5, 0.5] − 0.5 + [0.1, 0.0]	+0.5 × [2.5, 0.5] − 0.5 + [0.1, 0.0]
Transonic $1 < M_\infty < 1.5$	1.25 × Supersonic	1.25 × Supersonic

IV. InSight As-Flown Aerodynamic Performance

Flight performance was reconstructed from onboard inertial measurement unit accelerometer and rate gyro data. A more detailed discussion of the post-flight reconstruction and performance assessment for InSight is provided in Refs. [2] and [3]. Unlike Mars Science Laboratory, neither Phoenix nor InSight had any heatshield pressure instrumentation. For Phoenix and InSight, the aerodynamic performance cannot be separated from atmospheric conditions. InSight experienced higher than predicted acceleration and shorter than predicted flight time, landing 10 km uptrack and to the north of the targeted center of the predicted landing ellipse. While well within the design requirement, InSight experienced a peak deceleration exceeding 8 Earth g, slightly higher than the predicted maximum. The time from entry to touchdown was 41 s shorter than predicted.

The vehicle, though ballistic, trimmed at angles in excess of 4.8° during the hypersonic phase, shown in Fig. 7. The shaded regions in Fig. 7 define the conditions between the predicted bounded static instabilities. In looking at the attitude history within this shaded region, neither vehicle (InSight nor Phoenix) saw a significant reduction in trim attitude towards zero, implying this to be more of a region of static instability as opposed to the predicted pair of instabilities or an unintended non-zero radial CG offset. The peak trim α_T in both cases is nearly coincident with peak dynamic pressure during entry. Compared to Phoenix, InSight reached a higher trim α_T (4.8° versus 3.8°) and,

in general, flew with a larger α_T over the entire trajectory. It should be noted that the consistently non-zero attitude profiles, particularly between 5500 and 3800 m/s, for the non-spinning InSight and Phoenix entries are different from other ballistic Mars entries with spinning vehicles [5, 6, 8], suggesting spin-stabilization to be effective in reducing the impact of the static instability on hypersonic trim attitude.

Total angle of attack includes both angle of attack and angle of sideslip (see Fig. 2). Figure 7 shows the separate angles of attack and sideslip histories for InSight and Phoenix. While both vehicles flew with a similar sideslip history, InSight's angle of sideslip was nearly double that flown by Phoenix. Additionally, the angle of attack was negative for InSight, whereas Phoenix trimmed hypersonically at a positive angle of attack. When combined with the 180° bank angle for both vehicles, this translates into InSight trimming to a "lift-down" flight profile, contributing to the short timeline and uptrack landing location relative to prediction.

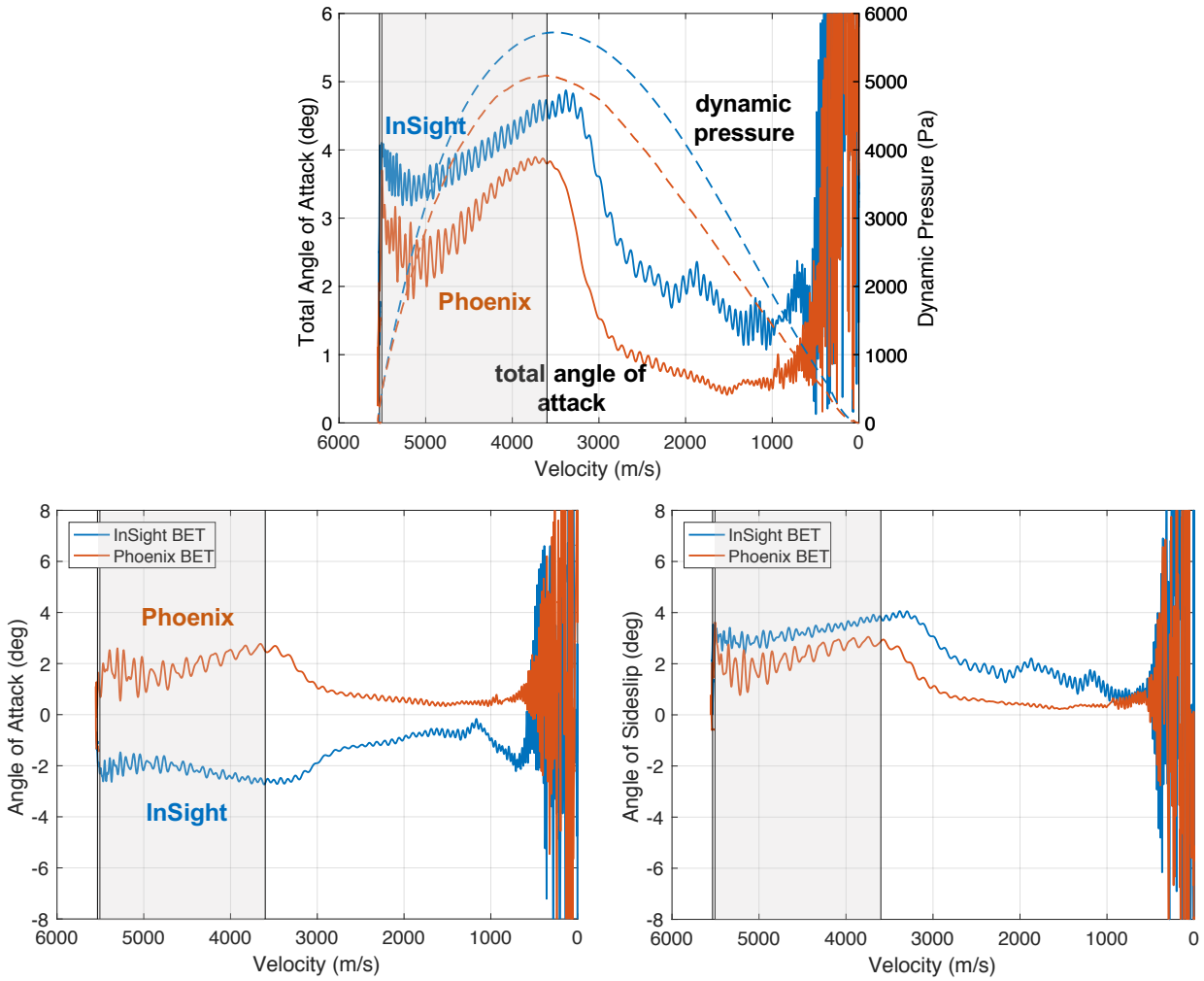

Fig. 7 Reconstructed attitude history from the Best Estimated Trajectory (BET).

Shown in Fig. 8, near peak dynamic pressure, the vehicle began to bank, uninitiated, as the vehicle was unguided, from 180° to near 35° by parachute deployment. Early in the entry phase, the reconstruction showed a reversal in the vehicle roll direction. With increasing dynamic pressure, the vehicle rolled clockwise (as seen from behind), but then changed to a counter-clockwise roll shortly after peak dynamic pressure. The initial clockwise roll rotated the vehicle's lift vector to the north, and when coupled with the large sideslip angle, is likely the primary contributor to the crossrange error in landing location. A similar roll reversal was observed for Phoenix but at an earlier point along the trajectory and with less correlation with dynamic pressure. With no pressure instrumentation on the vehicle, however, the cause of this behavior remains unknown.

While InSight did fly an onboard reaction control system (RCS), similar to Phoenix, the RCS was dead-banded within the atmosphere to avoid potentially adverse interactions and only fire if the vehicle experienced attitude rates of sufficient magnitudes as to endanger the vehicle. While the reconstructed attitude profile shows non-zero rates and angles, InSight did not have any RCS usage within the atmosphere.

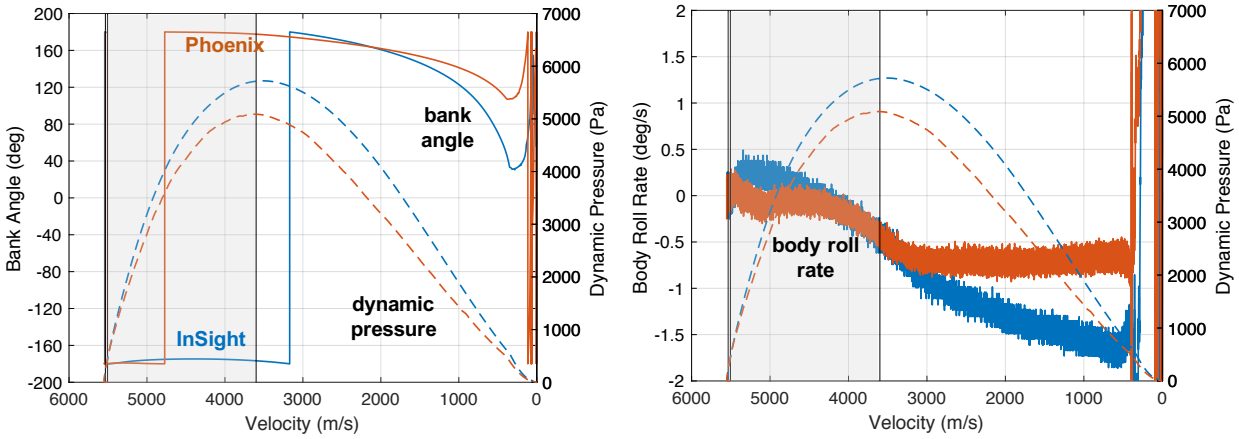

Fig. 8 Reconstructed bank angle and roll history.

Pitching moment and axial force coefficient uncertainties are the largest contributors to landing ellipse size. Along with local atmosphere conditions, these parameters contribute to departures from the nominal time of flight. Static instabilities were predicted in two regions along the reference trajectory: one near the non-continuum/continuum boundary and the other later in the hypersonic phase, between 3800 and 3300 m/s. These two static instabilities have been observed in the post-flight reconstruction of Mars Pathfinder (spin-stabilized), the Mars Exploration Rovers (spin-stabilized) [6, 8]. However, the InSight and Phoenix reconstructions indicate behavior more characteristic of a single instability region (see Fig. 7), suggesting that errors in the trim behavior from hypersonic non-equilibrium CFD solutions along the dynamic pressure pulse may have a more substantial impact on non-spinning, ballistic entry vehicle performance, if the vehicle can be considered to have trimmed at all.

An axisymmetric vehicle can trim to a non-zero angle of attack with a radial offset CG, as was used on the Viking landers, or through a non-symmetric pressure distribution. For InSight and Phoenix, there were no intentional offsets to the CG, and the shape is known to produce an unstable pressure distribution at certain hypersonic conditions within the Martian atmosphere. Figure 9 compares the reconstructed trim α_T history with the pre-flight predicted trajectory, as well as 3σ uncertainties on the radial center-of-gravity location, Z_{CG}, and pitching moment adder. These uncertainties, while they increase the peak α_T magnitude and shift the peak to a slightly lower velocity, do not produce behavior matching that reconstructed for InSight. Figure 10 shows the isolated effects of CG offset and C_m uncertainty on α_T. The reconstructed peak α_T occurred near 3400 m/s and is outside of the 3σ uncertainties on both CG offset and hypersonic C_m. The absence of distinct peaks in α_T and inconsistent offset between the reconstructed and predicted trim attitude profiles suggest that a constant offset CG is not the root cause of the observed flight behavior. While InSight experienced higher than expected deceleration loads during entry, and structural deformation could produce trim characteristics similar to those reconstructed, the reconstructed loads were still well below the design requirement for the aeroshell structure.

In addition to the aerodynamics described in this section, low density in the upper atmosphere also contributed to higher-than-expected deceleration and short EDL timeline for InSight [3]. Additionally, the direction of the lift vector and departures from zero degrees trim attitude are aerodynamic contributors to the as-flown performance for InSight. The crosstrack error to the north maps well to the roll direction of the vehicle as dynamic pressure increases along the trajectory, indicating the roll and not winds to be the likely driver.

V. Conclusions

InSight landed successfully on the surface of Mars in November 2018, flying a passive, non-spinning, ballistic trajectory. InSight and Phoenix exhibited similar behavior, primarily in terms of trim attitude and an uninitiated roll

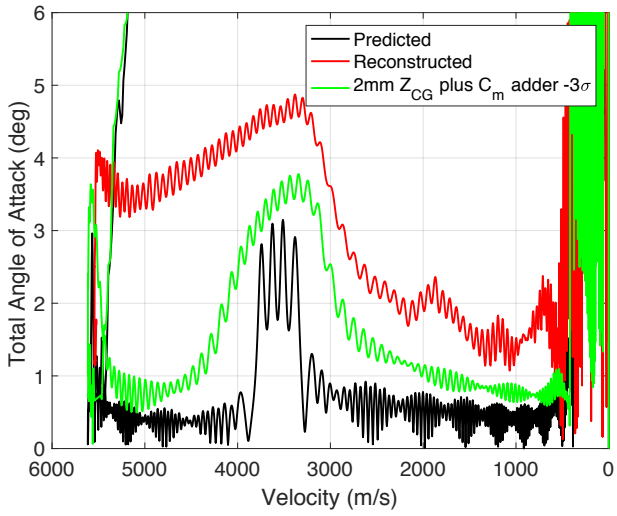

Fig. 9 Effect of 3σ CG offset and C_m adder uncertainty on α_T.

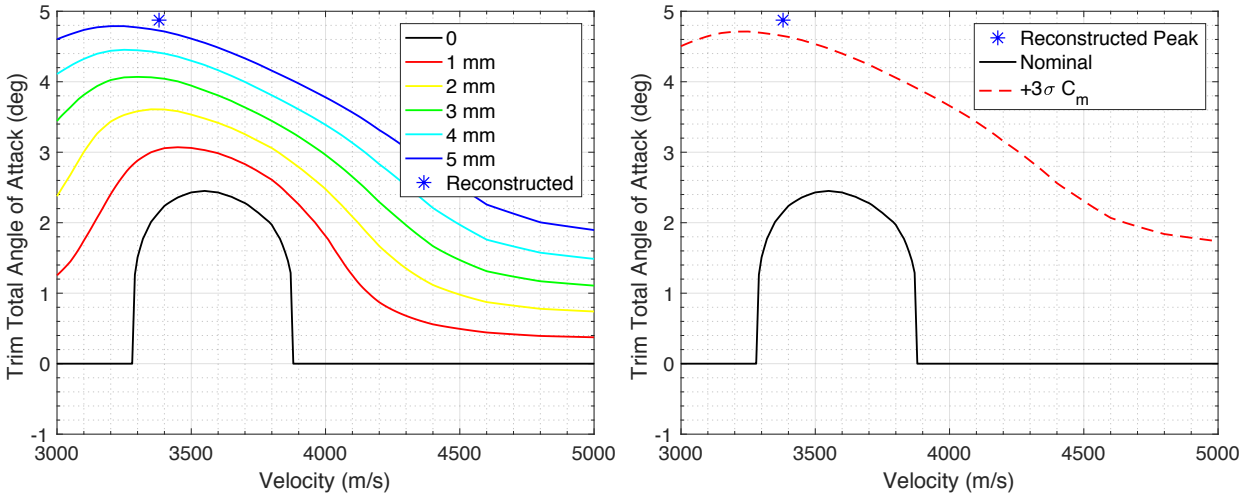

Fig. 10 Independent effects of CG offset and C_m uncertainty on α_{total}.

reversal correlated with dynamic pressure, though the behaviors observed for InSight were more severe. While the vehicle trimmed at a peak total angle of attack of 4.8° during the hypersonic phase of flight, no RCS firings were triggered within the atmosphere. The initial clockwise roll and non-zero trim angle of attack were significant contributors to the short timeline, larger-than-predicted deceleration loads, and the crosstrack and uptrack errors in landing. Without additional onboard instrumentation, such as the FADS suite flown on MSL, the exact cause(s) of the roll and trim attitude behavior reconstructed for InSight cannot be fully established.

References

[1] Hoffman, T., "InSight: Mission to Mars," *IEEE Aerospace Conference*, 2018. doi:10.1109/AERO.2018.8396723.

[2] Maddock, R. W., Cianciolo, A. M. D., Karlgaard, C. D., Korzun, A. M., Litton, D. K., and Zumwalt, C. H., "InSight Entry, Descent, and Landing Post-Flight Performance Assessment," AIAA Paper 2020–XXXX, January 2020.

[3] Karlgaard, C. D., Korzun, A. M., Schoenenberger, M., Bonfiglio, E. P., Kass, D. M., and Grover, M. R., "Mars InSight Entry, Descent, and Landing Trajectory and Atmosphere Reconstruction," AIAA Paper 2020–XXXX, January 2020.

[4] Dyakonov, A. A., Glass, C. E., Desai, P. N., and Van Norman, J. W., "Analysis of Effectiveness of Phoenix Entry Reaction Control System," *Journal of Spacecraft and Rockets*, Vol. 48, No. 5, 2011, pp. 746–755. doi:10.2514/1.40965.

[5] Edquist, K. T., Desai, P. N., and Schoenenberger, M., "Aerodynamics for Mars Phoenix Entry Capsule," *Journal of Spacecraft and Rockets*, Vol. 48, No. 5, 2011, pp. 713–726. doi:10.2514/1.46219.

[6] Schoenenberger, M., Cheatwood, F. M., and Desai, P. N., "Static Aerodynamics of the Mars Exploration Rover Entry Capsule," AIAA Paper 2005–0056, January 2005.

[7] McGhee, R. J., III, P. M. S., and Pelt, R. E., "Transonic Aerodynamic Characteristics of the Viking Entry and Lander Configurations," NASA TM X-2354, January 1971.

[8] Spencer, D. A., Blanchard, R. C., Braun, R. D., Kallemeyn, P. H., and Thurman, S. W., "Mars Pathfinder Entry, Descent, and Landing Reconstruction," *Journal of Spacecraft and Rockets*, Vol. 36, No. 3, 1999, pp. 357–366. doi:10.2514/2.3478.